Nanoscale Fresnel coherent diffraction imaging tomography using ptychography

I. Peterson,[1,3] B. Abbey,[2,3] C.T. Putkunz,[1,3] D.J. Vine,[4] G.A. van Riessen,[2,3], G.A. Cadenazzi,[1,3] E. Balaur,[2,3] R. Ryan,[1,3] H.M. Quiney,[1,3] I. McNulty,[4] A.G. Peele,[2,3] and K.A. Nugent[1,3,*]

[1]*School of Physics, University of Melbourne, Victoria 3010, Australia*
[2]*Department of Physics, La Trobe University, Victoria 3086, Australia*
[3]*Australian Research Council Centre of Excellence for Coherent X-Ray Science, Australia*
[4]*Advanced Photon Source, Argonne National Laboratory, Argonne, IL 60439, USA*
[*]*keithan@unimelb.edu.au*

Abstract: We demonstrate Fresnel Coherent Diffractive Imaging (FCDI) tomography in the X-ray regime. The method uses an incident X-ray illumination with known curvature in combination with ptychography to overcome existing problems in diffraction imaging. The resulting tomographic reconstruction represents a 3D map of the specimen's complex refractive index at nano-scale resolution. We use this technique to image a lithographically fabricated glass capillary, in which features down to 70 *nm* are clearly resolved.

OCIS codes: (340.7440) X-ray imaging; (340.7460) X-ray microscopy.

References and links

1. J. W. Miao, P. Charalambous, J. Kirz, and D. Sayre, "Extending the methodology of x-ray crystallography to allow imaging of micrometre-sized non-crystalline specimens," Nature **400**, 342–344 (1999).
2. K .A. Nugent, "Coherent methods in the x-ray sciences," Adv. Phys. **59**, 1–99 (2010).
3. H. N. Chapman, A. Barty, S. Marchesini, A. Noy, S. R. Hau-Riege, C. Cui, M. R. Howells, R. Rosen, H. He, J. C. H. Spence, U. Weierstall, T. Beetz, C. Jacobsen, and D. Shapiro, "High-resolution ab initio three-dimensional x-ray diffraction microscopy," J. Opt. Soc. Am. A. **23**, 1179–1200 (2006).
4. A. Barty, S. Marchesini, H. N. Chapman, C. Cui, M. R. Howells, D. A. Shapiro, A. M. Minor, J. C. H. Spence, U. Weierstall, J. Ilavsky, A. Noy, S. P. Hau-Riege, A. B. Artyukhin, T. Baumann, T. Willey, J. Stolken, T. van Buuren, and J. H. Kinney, "Three-dimensional coherent x-ray diffraction imaging of a ceramic nanofoam: Determination of structural deformation mechanisms," Phys. Rev. Lett. **101**, 055501 (2008).
5. Y. Nishino, Y. Takahashi, N. Imamoto, T. Ishikawa, and K. Maeshima, "Three-dimensional visualization of a human chromosome using coherent x-ray diffraction," Phys. Rev. Lett. **102**, 018101 (2009).
6. M. Dierolf, A. Menzel, T. Thibault, P. Schneider, C. M. Kewish, R. Wepf, O. Bunk, and F. Pfeiffer, "Ptychographic x-ray computed tomography at the nanoscale," Nature **467**, 436–439 (2010).
7. K. A. Nugent, A. G. Peele, H. M. Quiney, and H. N. Chapman, "Diffraction with wavefront curvature: a path to unique phase recovery," Acta Crystallogr. A **61**, 373–381 (2005).
8. G. J. Williams, H. M. Quiney, B. B. Dhal, C. Q. Tran, K. A. Nugent, A. G. Peele, D. Paterson, and M. D. de Jonge, "Fresnel coherent diffractive imaging," Phys. Rev. Lett. **97**, 025506 (2006).
9. B. Abbey, K. A. Nugent, G. J. Williams, J. N. Clark, A. G. Peele, M. A. Pfeifer, M. De Jonge, and I. McNulty, "Keyhole coherent diffractive imaging," Nat. Phys. **4**, 394–398 (2008).
10. B. Abbey, G. J. Williams, M. A. Pfeifer, J. N. Clark, C. T. Putkunz, A. Torrance, I. McNulty, T. M. Levin, A. G. Peele, and K. A. Nugent, "Quantitative coherent diffractive imaging of an integrated circuit at a spatial resolution of 20 nm," App. Phys. Lett. **93**, 214101 (2008).

#170239 - $15.00 USD Received 11 Jun 2012; revised 5 Sep 2012; accepted 18 Sep 2012; published 12 Oct 2012

11. G. J. Williams, E. Hanssen, A. G. Peele, M. A. Pfeifer, J. N. Clark, B. Abbey, G. A. Cadenazzi, M. D. de Jonge, S. Vogt, L. Tilley, and K. A. Nugent, "High-resolution x-ray imaging of plasmodium falciparum-infected red blood cells," Cytom. Part A **73A**, 949–957 (2008).
12. H. M. Quiney, A. G. Peele, Z. Cai, D. Paterson, and K. A. Nugent, "Diffractive imaging of highly focused x-ray fields," Nat. Phys. **2**, 101–104 (2006).
13. L. W. Whitehead, G. J. Williams, H. M. Quiney, K. A. Nugent, A. G. Peele, D. Paterson, M.D. de Jonge, and I. McNulty, "Fresnel diffractive imaging: Experimental study of coherence and curvature," Phys. Rev. B **77**, 104112 (2008).
14. R. Hegerl and W. Hoppe, "Dynamische theorie der kristallstrukturanalyse durch elektronenbeugung im inhomogenen primarstrahlwellenfeld," Ber. Bunsenges. Phys. Chem. **74**, 1148–1154 (1970).
15. J. M. Rodenburg and H. M. L Faulkner, "A phase retrieval algorithm for shifting illumination," App. Phys. Lett. **85**, 4795–4797 (2004).
16. P. Thibault, M. Dierolf, A. Menzel, O. Bunk, C. David, and F. Pfeiffer, "High-resolution scanning x-ray diffraction microscopy," Science **321**, 379–382 (2008).
17. A. Schropp, R. Hoppe, J. Patommel, D. Samberg, F. Seiboth, S. Stephan, G. Wellenreuther, G. Falkenberg, and C. G. Schroer, "Hard x-ray scanning microscopy with coherent radiation: Beyond the resolution of conventional x-ray microscopes," Applied Physics Letters **100**, 253112 –253112–3 (2012).
18. D. J. Vine, G. J. Williams, B. Abbey, M. A. Pfeifer, J. N. Clark, M. D. de Jonge, I. McNulty, A. G. Peele, and K. A. Nugent, "Ptychographic fresnel coherent diffractive imaging," Phys. Rev. A **80**, 063823 (2009).
19. C. T. Putkunz, M. A. Pfeifer, A. G. Peele, G. J. Williams, H. M. Quiney, B. Abbey, K. A. Nugent, and I. McNulty, "Fresnel coherent diffraction tomography," Opt. Express **18**, 11746–11753 (2010).
20. C. T. Putkunz, J. N. Clark, D. J. Vine, G. J. Williams, M. A. Pfeifer, E. Balaur, I. McNulty, K. A. Nugent, and A. G. Peele, "Phase-diverse coherent diffractive imaging: High sensitivity with low dose," Phys. Rev. Lett. **106**, 013903 (2011).
21. J. R. Fienup, "Phase retrieval algorithms: a comparison," Appl. Optics **21**, 2758–2769 (1982).
22. H. M. Quiney, K. A. Nugent, and A. G. Peele, "Iterative image reconstruction algorithms using wave-front intensity and phase variation," Opt. Lett. **30**, 1638–1640 (2005).
23. A. C. Kak and M. Slaney, *Principles of Computerized Tomographic Imaging* (Society for Industrial Mathematics, 1988).
24. I. McNulty, A. Khounsary, Y. P. Feng, Y. Qian, J. Barraza, C. Benson, and D. Shu, "A beamline for 1-4 kev microscopy and coherence experiments at the advanced photon source," Rev. Sci. Instrum. **67**, 3372 (1996).
25. D. J. Vine, G. J. Williams, J. N. Clark, C. T. Putkunz, M. A. Pfeifer, D. Legnini, C. Roehrig, E. Wrobel, E. Huwald, G. van Riessen, B. Abbey, T. Beetz, J. Irwin, M. Feser, B. Hornberger, I. McNulty, K. A. Nugent, and A. G. Peele, "An in-vacuum x-ray diffraction microscope for use in the 0.7-2.9 kev range," Rev. Sci. Instrum. **83**, 033703 (2012).
26. M. Born and E. Wolf, *Principles of Optics: Electromagnetic Theory of Propagation, Interference and Diffraction of Light (7th Edition)* (Cambridge University Press, 1999).
27. D. Shapiro, P. Thibault, T. Beetz, V. Elser, M. Howells, C. Jacobsen, J. Kirz, E. Lima, H. Miao, A. M. Neiman, and D. Sayre, "Biological imaging by soft x-ray diffraction microscopy," Proc. Nat. Acad. Sci. U.S.A. **102**, 15343–15346 (2005).
28. J. N. Clark, C. T. Putkunz, M. A. Pfeifer, A. G. Peele, G. J. Williams, B. Chen, K. A. Nugent, C. Hall, W. Fullagar, S. Kim, and I. McNulty, "Use of a complex constraint in coherent diffractive imaging," Opt. Express **18**, 1981 (2010).
29. R. G. Paxman, T. J. Schulz, and J. R. Fienup, "Joint estimation of object and abberations by using phase diversity," J. Opt. Soc. Am. A **9**, 1072–1085 (1992).
30. L. W. Whitehead, G. J. Williams, H. M. Quiney, D. J. Vine, R. A. Dilanian, S. Flewett, K. A. Nugent, A. G. Peele, E. Balaur, and I. McNulty, "Diffractive imaging using partially coherent x rays," Phys. Rev. Lett. **103**, 243902 (2009).
31. B. Abbey, L. W. Whitehead, H. M. Quiney, D. J. Vine, G. Cadenazzi, C. A. Henderson, K. A. Nugent, E. Balaur, C. T. Putkunz, A. G. Peele, G. J. Williams, and I. McNulty, "Lensless imaging using broadband x-ray sources," Nat. Phot. **5**, 420–424 (2011).

1. Introduction

The X-ray Coherent Diffractive Imaging (CDI) is a form of lensless imaging for which the resolution is not limited by the quality of the available X-ray optics [1,2]. The short wavelength and penetrating power of X-rays suggests it to be an excellent candidate for 3D nanoscale imaging for both the biological and materials sciences [3–6].

CDI typically illuminates a finite sample with a plane wave and the diffraction data is collected in the far-field, which is then used to reconstruct the specimens exit surface wave, usually

#170239 - $15.00 USD Received 11 Jun 2012; revised 5 Sep 2012; accepted 18 Sep 2012; published 12 Oct 2012

via iterative phase retrieval methods. A more recent approach illuminates the sample with a divergent spherical wave, overcoming many of the ambiguities and convergence problems in the image reconstruction process, while also removing the need for a central beam stop to block the undiffracted illumination. The use of a pre-characterised, curved illumination for CDI is known as Fresnel Coherent Diffractive Imaging (FCDI) [7–11]. The characterisation of the incident wavefield is obtained from a measurement of the illumination intensity without the sample in place [12]. FCDI has been shown to be a robust, unambiguous and quantitative method for recovering the complex transmission function of a specimen. In addition it has been demonstrated that the phase curvature in the incident beam yields an improved tolerance to partial coherence [13].

Ptychography is a technique that has attracted great interest due to the improvement it affords in the quality and achievable contrast in CDI images [14–17]. The method involves the collection of diffraction patterns using a finite illumination, each overlapping to some degree, then determining the phase and amplitude of the exit surface wave common to these overlap regions using iterative phase retrieval. The large amount of data acquired improves the reliability of the reconstruction and so provides a more robust and accurate imaging method. Two dimensional X-ray ptychographic FCDI was first demonstrated by Vine *et al.* [18], and a proof-of-principle FCDI tomography experiment in the optical regime has also been carried out [19]. The three dimensional extension of this method to X-ray wavelengths has significant implications for high-resolution *in situ* or *in vivo* imaging of biological specimens. It also provides an alternative to imaging using electrons or optical wavelengths where in many situations the thickness of specimen is better suited to the penetrating power and contrast mechanisms that X-ray wavelengths provide. Three dimensional plane wave X-ray CDI [3–5] has previously been combined with ptychography to produce tomographic reconstructions of a mouse femur [6]. In this paper we present a demonstration of ptychographic FCDI tomography in the X-ray regime.

2. Method

Two dimensional ptychographic FCDI has been described elsewhere [18, 20]. The benefits of adopting a curved beam approach in three dimensions are similar to those for two dimensional diffraction imaging. These include robustness to partial coherence in the illumination [13], improved convergence characteristics during phase retrieval [8], and high contrast and sensitivity when applying a minimal radiation dose [20]. Performing the experiment without a beamstop also makes it possible to record the low spatial frequency information which is lost in the analogous plane-wave experiment.

A discussion of how the curved beam diffraction imaging approach can be extended to three-dimensional imaging may also be found in Putkunz *et al.* [19]. The underlying aim of FCDI tomography is to reconstruct a series of two-dimensional projections of the sample and combine these to recover the full three-dimensional complex refractive index, defined as: $n(\boldsymbol{r}_s) = 1 - \delta(\boldsymbol{r}_s) + i\beta(\boldsymbol{r}_s)$. For a given projection, the transmission function $T_\theta(\boldsymbol{\rho}_s)$ is given by:

$$T_\theta(\boldsymbol{\rho}_s) = \exp\left[-ik\int_z \delta(\boldsymbol{\rho}_s, z) - i\beta(\boldsymbol{\rho}_s, z)dz\right] \tag{1}$$

where θ is projection angle, $k = 2\pi/\lambda$ and $\boldsymbol{\rho}_s$ is the planar sample coordinate. In the Born approximation, the transmission function is calculated from the recovered the exit surface wavefield (ESW) for a given projection via $\psi_\theta(\boldsymbol{\rho}_s) = \psi_0(\boldsymbol{\rho}_s)T_\theta(\boldsymbol{\rho}_s)$, where $\psi_0(\boldsymbol{\rho}_s)$ describes the illuminating wave. After recovering the complex illumination [12], the sample transmission function for each projection, given by Eq. (1), is recovered using CDI algorithms (specifically "error reduction" [21]) modified for an FCDI geometry [8]. In these algorithms the reconstructed illumination may be used to define the object extent [9].

#170239 - $15.00 USD Received 11 Jun 2012; revised 5 Sep 2012; accepted 18 Sep 2012; published 12 Oct 2012

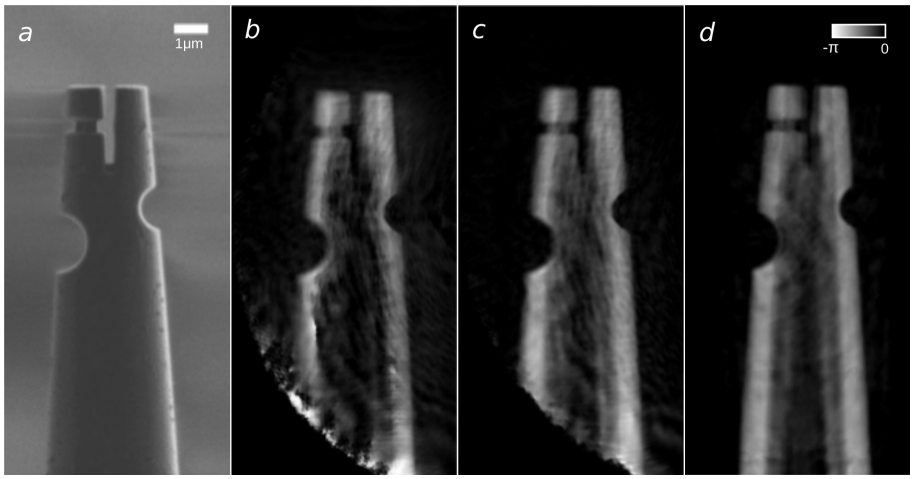

Fig. 1. (a) SEM image of the sample. Figures (b) and (c) show reconstructions of the transmission phase for the same non-ptychographic sample projection with bootstrap and without bootstrap input respectively. (d) A ptychographic reconstruction of the sample (scale bars are common to all reconstructions).

It has previously been shown [19] that "bootstrapping", a process in which a reconstruction is seeded with reconstructions from neighbouring projections, can improve the convergence speed of the algorithm and reduce image artefacts. In this study we use higher quality ptychographic FCDI reconstructions to provide the seeding reconstructions for neighbouring non-ptychographic FCDI projections. This can produce higher quality reconstructions for the non-ptychographic data sets while significantly reducing the radiation dose acquired compared to a ptychographic data acquisition. In FCDI the complex illumination provides a reference phase [8, 22] for each reconstruction. This means there is no phase offset between neighbouring projection reconstructions, and we are not required to remove this prior to the tomographic assembly process (in contrast to plane wave CDI tomography). Providing a sufficient number of projections are recovered, standard tomographic algorithms such as filtered back projection [23] may then be used to recover the three dimensional distribution of either δ or β within the specimen.

3. Experiment

The experiment was conducted at sector 2-ID-B at the Advanced Photon Source, Argonne National Laboratory [24] using the dedicated *in vacuo* FResnel Imaging END (FRIEND) endstation [25]. We used a 2.5 keV X-ray beam to coherently illuminate a 160 μm Fresnel zone plate (FZP) with nominal outer zone width of 50 nm, and placed the sample within the diverging illumination. At this energy the focal length is 16.4 mm. The combination of a central stop at the zone plate and an order sorting aperture (OSA) close to the focal plane block the zeroth order beam and isolate the first order focus. The sample was placed 1.2 mm downstream of the focus to provide an illumination approximately 12 μm in diameter in the object plane. The diffraction images were recorded 0.76 m downstream on a 2048×2048 cooled CCD with 13.5 μm square pixels. These were later cropped to a 1024×1024 array. The corresponding pixel size in the sample plane due to the numerical aperture of the detector is 27 nm. The actual resolution of the reconstructions is generally lower than this as it is dependent on the signal-to-noise ratio of the recorded diffraction patterns. Based on Abbe theory [26] and the numerical aperture, NA, of

#170239 - $15.00 USD Received 11 Jun 2012; revised 5 Sep 2012; accepted 18 Sep 2012; published 12 Oct 2012

the detector (defined here to be one half of the detector acceptance angle), we find a theoretical resolution limit of $\Gamma = 0.82\lambda/\mathrm{NA} \approx 44\,\mathrm{nm}$.

The sample was a glass capillary approximately $2.5\,\mu\mathrm{m}$ wide at the tip, shaped using a focussed ion beam. The region of interest measured on the sample is shown in the scanning electron microscope (SEM) image in Fig. 1(a). The tomographic data were acquired by rotating the sample in steps of 2° over a range of $0^\circ \leq \theta \leq 180^\circ$, collecting 6 frames per projection. In addition to this we also recorded 7 ptychographic data sets at 30° intervals over the full range of θ in order to facilitate "bootstrapping". Each ptychographic set consisted of 9 separate probe positions in a 3×3 grid, with 25 frames at each probe position. The sample was encompassed in the field of view for all probe positions resulting in a probe overlap fraction of 100 %. The exposure time per frame for all the data sets was 0.75 s. The combined exposure time for the specimen was approximately 1.2 hours. The average photon fluence on the sample per recorded data frame was $2.1 \times 10^5\,\mathrm{photons}/\mu\mathrm{m}^2$, providing a dose rate of $2.2 \times 10^4\,\mathrm{Gy}$ per tomographic projection, $8.1 \times 10^5\,\mathrm{Gy}$ per ptychographic position, and a total dose of approximately $7.5 \times 10^6\,\mathrm{Gy}$.

4. Results

An example reconstruction for a single projection is provided in Fig. 1(b). The capillary wall thickness of 350 nm was measured from the reconstructions; a parameter that cannot be determined from the SEM image. Surface charge effects result in "shadowing" at the capillary edge in the SEM image, not suggestive of any real features, hence these are not present in the FCDI reconstructions in Fig. 1. Using the convention that the resolution is given by the point where the phase-retrieval transfer function (PRTF) drops to 1/e [27] provides a resolution estimate for the reconstructed transmission function of 42 nm. This compares to the result from a Power Spectral Density (PSD) analysis of 35 nm. As a further method for estimating resolution, a sigmoidal function was fitted to a hard edge in the reconstructed transmission function of the capillary and averaged over 20 projections [10]. This method targets a specific feature and is therefore unaffected by systematic artefacts which may appear as features when using other methods. The full width at half maximum of the derivative of this function provides an upper-bound estimate of 70 nm for the resolution achieved in the reconstructions.

Ptychographic FCDI reconstructions were used to seed or "bootstrap" [19] successive projections. This method was applied in steps of 2° over a range of $\pm 15^\circ$ from each ptychographic projection. The advantage of this bootstrapping approach may be appreciated by comparing the seeded and unseeded reconstructions in Fig. 1(a) and 1(b) respectively. We note in particular the improved uniformity in the capillary wall, as well as the reduced artefacts in the central, weaker regions of the projected transmission function. The low frequency information carried by the holographic region means that these reconstructions were able to be performed with just 500 iterations. Extraneous high-angle scatter from the OSA is thought to be largely responsible for the azimuthal artefacts present in the single position reconstructions.

A total of 90 seeded projections were used to reconstruct the three-dimensional complex sample transmission function using the filtered back-projection algorithm. A single tomographic slice through the full 3D reconstruction is shown in Fig. 2(a). The protrusion, highlighted by the red circle is present in both the adjacent slices and in the final 3D reconstruction. The final 3D result is shown as a surface rendering in Fig. 2(b) and 2(c). The etched features of the capillary, also visible in the SEM are clearly defined. In addition some extruded material (marked by the red circle in 2d) due to errors in the etching process is also visible. The appearance of these features, which are also visible in the SEM image shown in Fig. 2, further demonstrate the ability of the technique to resolve nanoscale features. In general the process of reconstructing a three-dimensional image from a set of projections is expected to produce a lower resolution

#170239 - $15.00 USD Received 11 Jun 2012; revised 5 Sep 2012; accepted 18 Sep 2012; published 12 Oct 2012

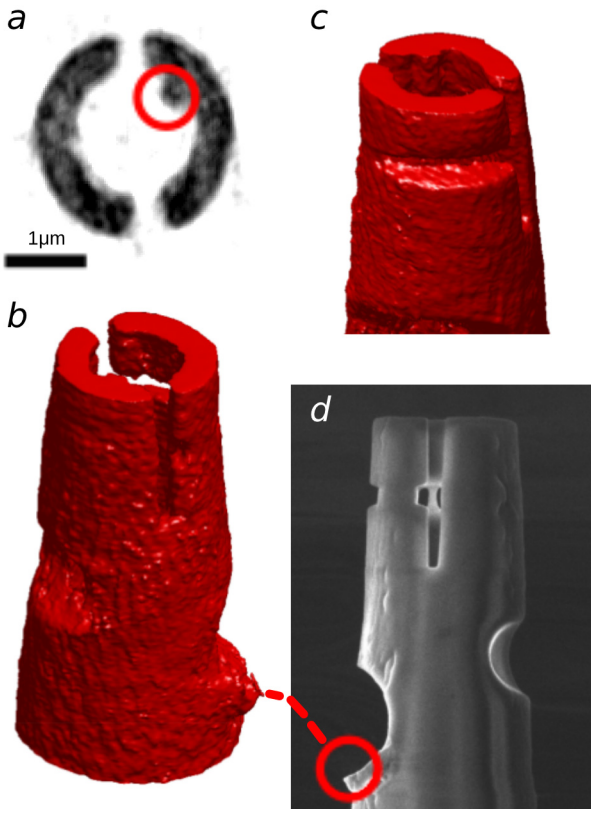

Fig. 2. (a) Tomographic slice through the upper region of the tomographic reconstruction surface rendered in (b) and (c). The internal protrusion highlighted within the red circle is a ridge running through the tip interior. (d) an SEM image shows the extrusion in (b) circled in red.

image than the individual two dimensional projections. It has also been well-established in the literature [8] that CDI offers a significant improvement in terms of spatial resolution over STXM. Finally, experimentally, the FWHM of the zone plate focal spot is usually $10-20\%$ larger than the nominal outer zone width. Hence, we believe the images presented are an improvement over the equivalent three-dimensional STXM image that would be obtained.

Analysis of tomographic slices allows one to quantitatively determine components of the 3D refractive index, $n(\boldsymbol{r}_s)$. This is possible because in FCDI the two dimensional complex transmission function, under the projection approximation, can be explicitly calculated from the exit wave of the specimen [28]. As described in Eq. (1) the phase, ϕ, and amplitude, $|T|$, of the recovered transmission function are then related to the components of the refractive index via:

$$\begin{aligned} \phi &= -k\int_z \delta(\boldsymbol{\rho}_s,z)dz \\ ln(|T|) &= k\int_z \beta(\boldsymbol{\rho}_s,z)dz \end{aligned} \tag{2}$$

hence filtered back projection using either ϕ or $ln(|T|)$ will yield refractive index components

#170239 - $15.00 USD Received 11 Jun 2012; revised 5 Sep 2012; accepted 18 Sep 2012; published 12 Oct 2012

δ and β respectively. Accordingly, the tomographic reconstruction shown in Fig. 2 results in a mean value of $\delta = (5.85 \pm 1.40) \times 10^{-5}$. This was calculated by generating a histogram of the reconstructed voxels and analysing the distribution. The refractive index of typical borosilicate glass at this energy, with a density of $2.3\,\mathrm{g/cm^3}$, gives theoretical values $\delta = 7.63 \times 10^{-5}$ and $\beta = 3.79 \times 10^{-6}$. The measured δ agrees with the expected value. At this energy the dominant interaction of the specimen with the incident illumination (and hence dominant contrast mechanism) in the specimen is the phase interaction. The amplitude of the reconstructed transmission function for each projection was of accordingly lower quality and resulted in an unreliable prediction for β. This is confirmed by considering the expected transmission based on the theoretical value of β, predicting a transmission of at most 7%.

We believe the fine scale oscillations in 3D reconstructions are due to slight misalignment of the tomographic projections, difficult without fiducial markers, time variation in the illumination and high angle OSA scatter. In FCDI the cost of increased algorithmic stability is a high sensitivity to both sample stability [8] and changes in the experimental geometry through sample excursions. Artefacts are therefore introduced due to the precession of the sample about the rotational axis. The circle of confusion associated with sample excursion during the tomographic data acquisition had a radius of approximately $25\,\mu$m. Although corrections for this were applied in the reconstruction algorithm, the accumulated error of the uncertainty on the sample to focus distance inevitably had an impact on the reconstruction quality. Modification to the mechanical alignment system will further eliminate residual artefacts in the reconstruction and result in an increase in reconstruction quality. A time varying illumination and OSA scatter cause artefacts both in the white field subtraction in reciprocal space and the white field division in real space. These artefacts are greatly reduced in the ptychographic reconstructions as the oscillations are inconsistent between ptychographic positions and are therefore averaged out. Increasing the ratio of ptychographic to non-ptychographic projections, reconstructing projections for a larger number of angles and employing new variants on the ptychographic algorithm such as incorporating other forms of "phase diversity" [20, 29] would help to address these issues.

5. Conclusion

In this paper we have demonstrated X-ray FCDI tomography. Unlike existing planar tomographic CDI methods the technique is quantitative since the reconstructed complex illumination provides an absolute reference for the sample reconstructions. In addition, FCDI tomography can image three-dimensional sections of extended objects using data that contains a single measurement per projection with the inclusion of a nominal number of projections recovered via FCDI ptychography. A significant improvement in the quality and sensitivity of the reconstruction was observed through periodic "bootstrapping" using ptychographic FCDI. Comparison with a data set obtained through purely ptychographic FCDI tomography shows a tenfold reduction in the dose rate. This method lays the foundation for performing X-ray FCDI tomography on a range of biological and materials science samples and will thus find immediate application in the area of high-resolution three-dimensional X-ray microscopy. By utilising recent developments in the area of partially coherent CDI we expect to dramatically reduce the time for data collection allowing comparative studies of large numbers of similar samples to be performed [30, 31].

Acknowledgments

The authors acknowledge support from the Australian Research Council Centre of Excellence for Coherent X-ray Science. We acknowledge travel funding provided by the International Synchrotron Access Program (ISAP) managed by the Australian Synchrotron and funded by the

Australian Government. Use of the Advanced Photon Source is supported by the U.S. Department of Energy, Office of Science, and Office of Basic Energy Sciences, under Contract No. DE-AC02-06CH11357.

#170239 - $15.00 USD Received 11 Jun 2012; revised 5 Sep 2012; accepted 18 Sep 2012; published 12 Oct 2012